Mapping the Photoresponse of the Quantum-Dot Based Photon-Number-Resolving Detector

Trevor Geerdts,[a] Connor Govin,[b] and Eric Gansen

Department of Physics, The University of Wisconsin – La Crosse, 1725 State St, La Crosse, WI 54601, USA

[a]Corresponding author: geerdts.trevor@uwlax.edu
[b]connorpgovin@gmail.com

Abstract. Efficient and versatile photon-number resolving detectors are critical to the development of future communication systems. The quantum-dot, optically-gated, field-effect transistor (QDOGFET) is one such detector. Utilizing quantum dots (QDs), tiny islands of semiconductor, imbedded in a transistor, QDOGFETs have been shown to exhibit single-photon sensitivity and photon-number-resolving (PNR) capabilities. A photon is detected when it photocharges a QD, which alters the amount of current flowing through the transistor by screening the gate field. Crucial to the resolving power is that each charged QD produce the same response, regardless of its location within the active area of the device. Here, we investigate the extent spatial nonuniformities in the QDOGFET's response to light limit its ability to distinguish different numbers of photons. By using an optical-scanning microscope (OSM), contour plots of a QDOGFET's response are acquired that show that the device exhibits localized "hotspots" where it is particularly sensitive to photons. The spatial resolution of the microscope is enhanced by capping the QDOGFET with a solid-immersion lens (SIL). We present experimental results that show how the hotspots depend on bias conditions and help decipher the root cause of the nonuniformities.

Introduction

This research is on the study of a novel method of detecting individual photons that makes use of nanometer-sized islands of semiconductor material, referred to as quantum dots (QDs). In a specially designed transistor, referred to as a QDOGFET (quantum dot, optically gated, field-effect transistor) [1-6], an array of QDs is embedded near the transistor's conductive channel. A photon is detected when it photocharges a QD, which alters the amount of current flowing through the transistor by screening the gate field. It has been demonstrated that QDOGFETs exhibit single-photon sensitivity with high internal quantum efficiency [1, 2] and, moreover, can accurately discriminate between the detection of 0, 1, 2, and 3 photons 83% of the time [3, 4]. However, it has also been shown that the resolving power of the detectors degrade as photon number increases, limiting the counts to low numbers. The physical mechanism that causes the degraded photon-number resolution is not well understood but appears to be related to variations in the response of the detector associated with the seed point of the photon. In this work, we present the results of measurements where we use an optical scanning microscope (OSM) and a solid-immersion lens (SIL) to investigate the spatial uniformity of the QDOGFET's response to light and use the results to identify the mechanisms that degrade the resolving power the device.

Background

QDOGFETs employ photoconductive gain [7] and QDs to detect individual photons. Figure 1(a) is a surface image of the device. The structure consists of alternating layers of GaAs and AlGaAs with a single layer of InGaAs QDs at the GaAs/AlGaAs interface, as shown in Fig. 1(b). A thin layer of silicon-doped material (Si δ-doping) provides excess electrons to the conduction band (CB), forming a two-dimensional electron gas (2DEG) at the GaAs/AlGaAs interface adjacent to the QDs. The detector is fabricated by depositing source and drain ohmic

contacts on the structure surface, etching a mesa between the contacts, and depositing a semitransparent platinum (Pt) Schottky-barrier gate across the mesa. The area where photons are detected is defined by the gated portion of the channel mesa, which for the QDOGFET studied in this work, is 5.625 μm^2 in area and encompasses about 2000 QDs.

The principles of operation of the QDOGFET are shown in Fig. 1(b). During operation, a reverse bias (negative gate voltage, V_g) is applied to the gate. When a photon is absorbed in the 100-nm-thick GaAs absorption layer (between the QDs and 2DEG), it excites an electron from the valence band (VB) to the conduction band (CB) leaving behind an empty state, or hole, in the VB. Subsequently, the positively charged hole is swept by the internal electric field toward the QDs, where it is trapped, while the excited electron is swept into the 2DEG. Once in a QD, the hole screens the internal field produced by the gate contact, subsequently changing the amount of current flowing in the 2DEG (ΔI_{ds}) for as long as the hole is stored in the dot. The magnitude of the step in current is dictated by the transconductance g_m of the FET, where care must be taken that the device is operating in the linear transconductive region. These current changes are converted to voltage changes, $\Delta V_{out} = -R\Delta I_{ds}G$, via a transimpedance amplifier with resistance, R, and gain, G, which are monitored by external electronics. During operation, the QDOGFET and its surrounding circuitry are cooled in order to decrease electrical noise.

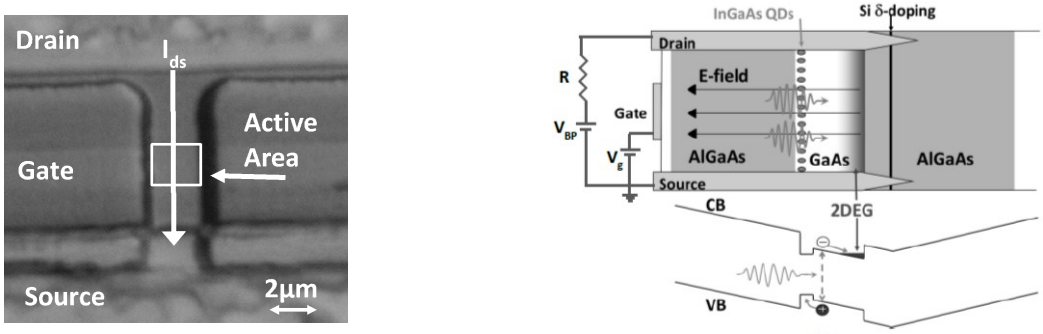

(a) (b)

FIGURE 1. (a) Image of the QDOGFET surface showing the drain, gate, source, active area, and conventional current direction during operation. (b) Schematic diagram of the composition and band structure of the QDOGFET.

When the gate and 2DEG of the QDOGFET are modelled as conductive plates of an ideal parallel-plate capacitor (PPC) with the QD layer treated as an infinite plane of charge storage, a concise relationship exists between the electrical and structural characteristics of the device and its photoresponse ΔI_{ds}. In the small-signal limit, the step in the channel current caused by a single trapped hole is given by

$$\Delta I_{ds} = g_m \frac{eW}{\varepsilon' A} \tag{1}$$

where e is the elementary charge, W is the distance between the Pt gate and the QD layer, ε' is the electric permittivity, and A is the active area [4, 8]. Although these current changes are small, over time even a single trapped hole causes a large change in the cumulative charge transferred in the 2DEG. The photoconductive gain associated with this process provides the detector with single-photon sensitivity. In addition, in the event that multiple photons photocharge multiple QDs, the net change in current is proportional to the number of photons, provided that each charged QD produces the same response regardless of its location within the active area of the detector. It is this aspect of the QDOGFETs that provides them with photon-number-resolving capabilities and is the focus of this work.

Experimental Procedure

The uniformity of the responses produced by different QDs within the QDOGFET was investigated using the cryogenic OSM shown schematically in Fig. 2(a). In these measurements, the SIL-capped QDOGFET was cooled to ~117 K while focussed 50-ns laser pulses were roster scanned over a 100-point grid, covering its active area. At each point on the grid, the individual steps in the output voltage, ΔV_{out}, caused by 200 laser pulses were recorded. The spatial resolution of the OSM was enhanced by mounting a cubic-zirconia SIL on the QDOGFET surface. The

diffraction limited spot diameter of monochromatic light is given by $\frac{0.522\lambda}{NA\,n}$, where λ is the wavelength of light, n is the index of refraction of the medium, and NA is the numerical aperture of the objective lens. As a result, by using a cubic-zirconia SIL with n = 2.14, the spot size was reduced by about half in comparison to what it would have been for a bare QDOGFET. The OSM utilized a 50x-magnification objective lens with a 13-mm working distance and NA=0.55, resulting in a diffraction limited spot size of 360nm. The actual spot diameter of the OSM was slightly larger due to imperfections within the system. Figure 2(a) shows the ideal case when the laser light is normally incident on the SIL. During scanning, deviation from this ideal case occurs as the laser spot moves over the surface of the SIL. However, the SIL has a diameter of 1mm, while the maximum dimension of our scanned area is less than 3µm. As these lengths differ by 3 orders of magnitude, any distortion effects due to scanning across the SIL are negligible.

From the roster scans of ΔV_{out}, contour plots of the mean step height (MSH), the mean number of photons (MNP), and the mean signal per photon (MSP) were produced using the statistical approach detailed in Ref. [2]. These contour plots were then superimposed onto a surface image of the device for reference. For example, a contour plot of the MSH is shown in Fig 2(b) for V_g = -0.5 V, V_{BP} = +2 V, R = 100kΩ, and G = 100. Variations in the response of the QDOGET are apparent in the data, where a "hotspot" consisting of a region of enhanced MSH is observed towards the drain side of the device. In the Results Section of this work, we present contour plots acquired for a variety of bias conditions that show how the hotspot depends on V_g and V_{BP}. From these data sets, we gain insight into what is causing the signal nonuniformity. Circuit parameters, R and G are kept constant for all measurements presented in this work.

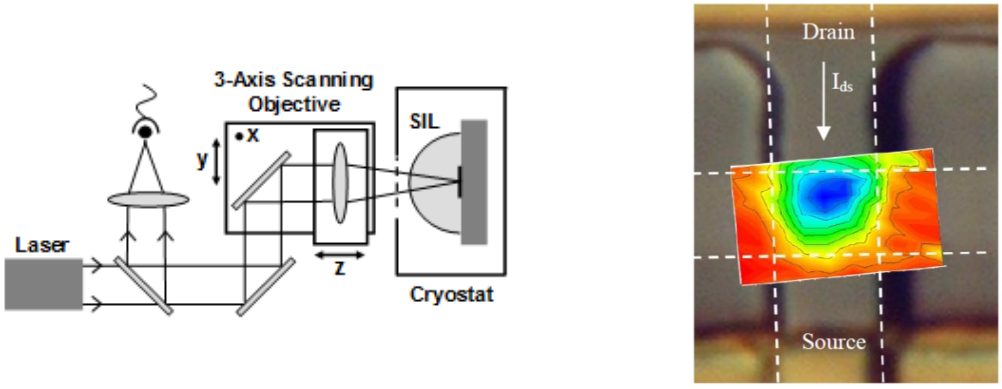

(a) (b)

FIGURE 2. (a) Schematic diagram of the OSM with SIL integration that was used to map the photo-response of QDOGFETs. (b) Overlay of a MSH contour plot, acquired for V_{BP} = +2V and V_g = -0.5 V, on an image of sample, with the active area outlined in dashed lines. For $V_{BP} > 0$, the drain potential is higher than the source potential, resulting in channel current I_{ds} flowing from drain to source.

RESULTS

Contour plots showing the effect of changing the direction of the channel current are shown in Fig. 3. In Fig. 3(a), V_{BP} = +2V, and I_{ds} flows in the downward direction, while in Fig. 3(b), V_{BP} = -2V, and I_{ds} flow in the upward direction. The bottom panels of the figure show the MSH for the entire 100-pt grid, where the active area of the device is indicated by black dashed lines. The top panels show the MNP, and the middle panels show the MSP. For these panels, data is only shown in and around the active area, since calculations of MNP and MSP are nonsensical beyond the boundaries of the active area where the QDOGFET is not sensitive to light. The theoretical value for the signal per photon, ΔV_{out}, calculated using Eqn. [1] is also provided in the figure for comparison. It is also marked by a black bar on the MSP legends. The potential difference between the source and drain contacts is also indicated on the figure.

The contour plots shown in Fig. 3 illustrate that the cause of the hotspot is electrical in nature, as opposed to being structural. Notice that for both polarities, the hotspot in the MSH (bottom panels) is observed near the

high-potential side of the gate. This would not be observed if the hotspot were due to variation in the thickness of the gate contact. The MNP and MSP data provide further insight into the origins of the hotspot. The MSP contour plots (middle panels) show some nonuniformity across the active area, but the pattern is less organized than the MSH data. Overall, the MSP measured across the majority of the active area is in good agreement with that predicted by the PPC model for both polarities. By contrast, the nonuniformity observed in the MNP contour plots (top panels) better match those observed for the MSH plots, which indicates that hotspot is a result of more efficient detection of photons seeded near the high-potential side of the active area.

The enhanced detection efficiency observed near the high-potential side of the active area can be explained by the dynamics of the photo-excited holes. While the transport of the holes perpendicular to the plane of the absorption layer is subject to the gate field, the motion of the holes in the plane of the absorption layer is influenced by the potential difference between the source and drain contacts. As such, positively charged holes tend to be "washed" downstream in the direction of the channel current I_{ds}. Given these dynamics, holes excited towards the high-potential side of the active area flow in the direction of I_{ds}, but can still be trapped by QDs beneath the gate contact and thus alter the channel current. By contrast, holes generated near the low-potential side of the active area tend to exit the gated area before they can be trapped by a QD.

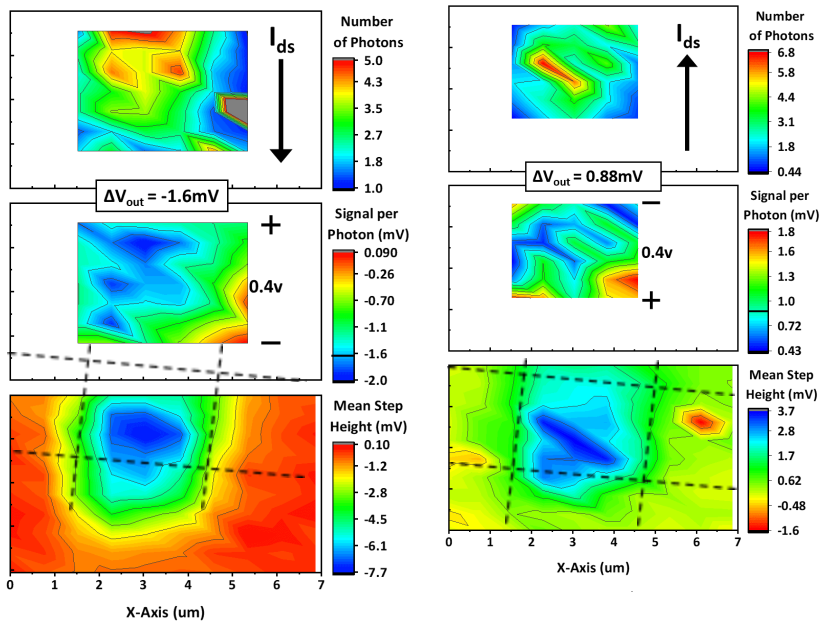

FIGURE 3. Contour plots of the MSH (bottom), MSP (middle), and MNP (top) for V_g = -0.5 V and (a) V_{BP} = +2V, and (b) V_{BP} = -2V. The signal per photon (ΔV_{out}) calculated using the PPC model and Eqn. [1] is provided for comparison. The potential difference between the source and drain contacts is provided in the middle panel.

The effects of varying V_g on the contour plots of the MSH, MNP, and MSP are shown in Fig. 4. The bottom panels show that the hotspot is more centrally located on the active area when a lower-magnitude gate voltage is used. As the magnitude of V_g is increased, the hotspot is pushed further towards the high-potential side of the active area. Also, the MSP becomes less uniform and deviates further from the theoretical ΔV_{out}. This behaviour can be explained by the large potential gradient that is formed across the active area when a large gate voltage is used. Notice that for V_g = -1.5V, the potential difference between the source and drain contacts is 0.85V, which results in a large gradient in the localized gate voltage over the active area of the device. While the 2DEG located on the low-potential side of the active area is gated by a local V_g of -1.5V, the other side is gated by a -2.35V bias. Holes trapped in QDs on the high-potential side of the active area will screen the larger gate field, which has a bigger impact on the channel current, consistent with the contour of the MSP data shown in Fig. 4(c). The fact that the

MNP is lower on the high-potential side of the active area indicates that although the MSP is enhanced in this region, the detection efficiency is low since most of the photoexcited holes drift out of the area downstream.

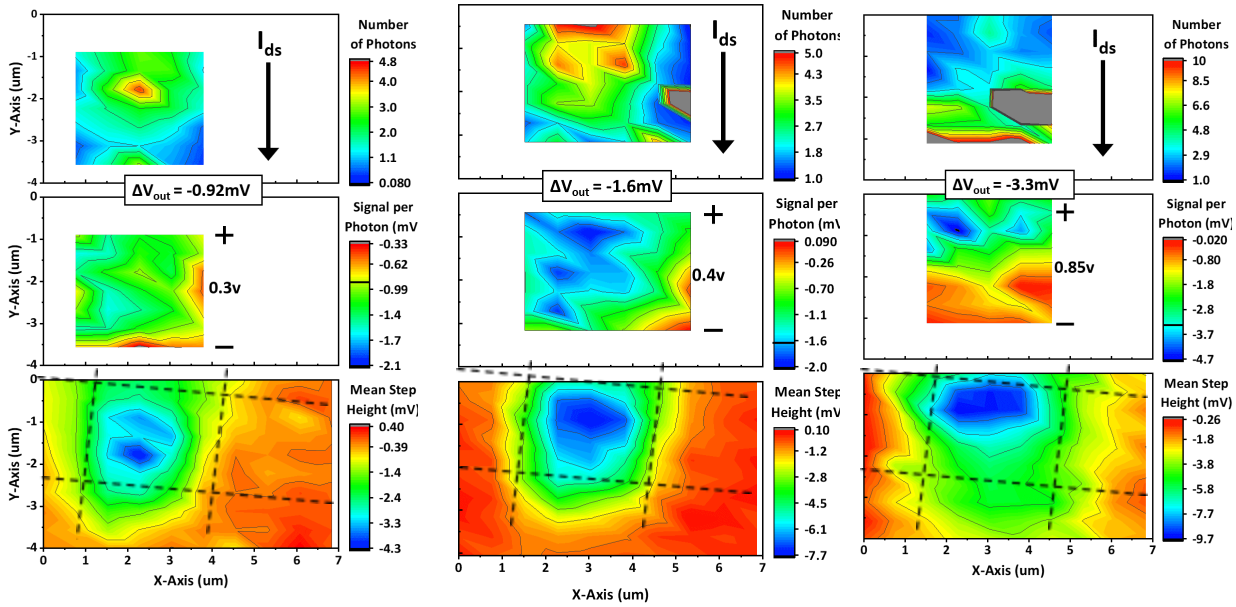

(a) (b) (c)

FIGURE 4. Contour plots of the MSH (bottom), MSP (middle), and MNP (top) for V_{BP} = +2V and (a) V_g = -0.1 V, (b) V_g = -0.5V, and (c) V_g = -1.5V. The signal per photon (ΔV_{out}) calculated using the PPC model and Eqn. [1] is provided for comparison. The potential difference between the source and drain contacts is provided in the middle panel.

Conclusions

In this work we have spatially resolved the variation in the MSH, MNP, and MSP over the active area of a SIL-capped QDOGFET. We have shown that the observed variation is due to electrical aspects of the device, rather than physical ones and that the gate voltage and current polarity greatly affect these variations. Specifically, the hotspot tends towards the high potential side of the active area, with a larger potential gradient corresponding to a greater shift to that side. The variation in the MNP can be explained in terms of the in-plane transport of the holes, where they tend to drift downstream in the same direction of I_{ds}. We also see that the MSP is more uniform for smaller gate voltages due to the lower localized potential difference over the active area. This finding is consistent with previous work [3, 4], where lower gate voltages were used when demonstrating the photon-number-resolving capabilities of QDOGFET.

Acknowledgements

We would like to acknowledge M. A. Rowe, S. M. Etzel, T. E. Harvey, and R. P. Mirin who were responsible for the epitaxial growth and fabrication of the structures studied in this work. This material is based upon work supported by the National Science Foundation, USA, under Grant No. 1406665. We would also like to thank the Wisconsin Space Grant Consortium, which provided funding through their Seed Grant.

References

1. M.A. Rowe, E.J. Gansen, M. Greene, R.H. Hadfield, T.E. Harvey, M.Y. Su, S.W. Nam, and R.P. Mirin, Appl. Phys. Lett. **89**, 253505 (2006).

2. E.J. Gansen, M.A. Rowe, M.B. Greene, D. Rosenberg, T.E. Harvey, M.Y. Su, R.H. Hadfield, S.W. Nam and R.P. Mirin, IEEE. J. Sel. Topics Quantum Electron, **13**, 1-11 (2007).
3. E.J. Gansen, M.A. Rowe, M.B. Greene, D. Rosenberg, T.E. Harvey, M.Y. Su, R.H. Hadfield, S.W. Nam and R.P. Mirin, Nature Photonics **1**, 585-588 (2007).
4. M.A. Rowe, E.J. Gansen, M.B. Greene, D. Rosenberg, T.E. Harvey, M.Y. Su, R.H. Hadfield, S.W. Nam, and R.P. Mirin, J. Vac. Sci. Technol. B **26**, 1174-1177 (2008).
5. M.A. Rowe, G.M. Salley, E.J. Gansen, S.M. Etzel, S.W. Nam, and R.P. Mirin, J. Appl. Phys. **107**, 63110 (2010).
6. E.J. Gansen, M.A. Rowe, S.D. Harrington, J.M. Nehls, S.M. Etzel, S.W. Nam and R.P. Mirin, J. Appl. Phys. **114**, 93103 (2013).
7. A. Rose, *Concepts in Photoconductivity and Allied Problems* (Interscience, New York, 1963), ch. 1.
8. G. Yusa and H. Sakaki, Electron. Lett. **32**, 491-493 (1996).